α-Synuclein Disrupts Vesicle Fusion by Two Mutant-Specific Mechanisms

Gyeongji Yoo[1], Hyeong Jeon An[2], Sanghun Yeou[1], and Nam Ki Lee[1,*]

[1]Department of Chemistry, Seoul National University, Seoul 08826, Korea, [2]Department of Physics, Pohang University of Science and Technology, Pohang 37673, Korea
*Correspondence: namkilee@snu.ac.kr
https://doi.org/10.14348/molcells.2022.0102
www.molcells.org

Synaptic accumulation of α-synuclein (α-Syn) oligomers and their interactions with VAMP2 have been reported to be the basis of synaptic dysfunction in Parkinson's disease (PD). α-Syn mutants associated with familial PD have also been known to be capable of interacting with VAMP2, but the exact mechanisms resulting from those interactions to eventual synaptic dysfunction are still unclear. Here, we investigate the effect of α-Syn mutant oligomers comprising A30P, E46K, and A53T on VAMP2-embedded vesicles. Specifically, A30P and A53T oligomers cluster vesicles in the presence of VAMP2, which is a shared mechanism with wild type α-Syn oligomers induced by dopamine. On the other hand, E46K oligomers reduce the membrane mobility of the planar bilayers, as revealed by single-particle tracking, and permeabilize the membranes in the presence of VAMP2. In the absence of VAMP2 interactions, E46K oligomers enlarge vesicles by fusing with one another. Our results clearly demonstrate that α-Syn mutant oligomers have aberrant effects on VAMP2-embedded vesicles and the disruption types are distinct depending on the mutant types. This work may provide one of the possible clues to explain the α-Syn mutant-type dependent pathological heterogeneity of familial PD.

Keywords: alpha-synuclein, familial mutant, Parkinson's disease, VAMP2, vesicle fusion

INTRODUCTION

Parkinson's disease (PD) is one of the prevalent neurodegenerative diseases, affecting more than 10 million people worldwide (Lee et al., 2022; Selvaraj and Piramanayagam, 2019). Aggregation of the α-synuclein (α-Syn) protein is considered to be a major culprit in the development of the disease (Goedert, 2001; Ross and Poirier, 2004; Spillantini et al., 1997; Yoo et al., 2022). α-Syn is an intrinsically disordered protein which is especially abundant in presynaptic terminals (Iwai et al., 1995; Maroteaux et al., 1988; Murphy et al., 2000). Although aggregates of α-Syn, called Lewy bodies, are the pathological hallmark of PD (Spillantini et al., 1997; 1998; Wakabayashi et al., 1997), the exact role of α-Syn in the pathogenesis of PD has yet to be fully deciphered. While most cases of PD are idiopathic, several mutations in the SNCA gene coding α-Syn, including A30P, E46K, and A53T, have been identified to cause early-onset familial PD (Kruger et al., 1998; Polymeropoulos et al., 1997; Zarranz et al., 2004).

α-Syn can be divided into three regions: the N-terminal region (residues 1-60), which is responsible for binding to membrane lipids; the nonamyloid-β component (residues 61-95), which is involved in forming fibrils with β-sheet structures; and the C-terminal region (residues 96-140), which is capable of interacting with the SNARE protein VAMP2 (vesicle-associated membrane protein 2, also called synaptobrevin-2) on synaptic vesicles (Burre et al., 2010; Sun et al., 2019).

Since all identified mutations of α-Syn are located in the N-terminal region, the interactions of α-Syn mutants with membrane lipids have been intensively studied (Robotta et al., 2017; Rovere et al., 2019; Tsigelny et al., 2012; Volles and Lansbury, 2002; Zakharov et al., 2007). Indeed, the association of α-Syn with membrane lipids is critical for its physiological function in presynaptic terminals (Burre et al., 2014; Fusco et al., 2016; Jo et al., 2000; Lou et al., 2017). α-Syn assembles metastable helical multimers, predominantly tetramers when bound to lipid membranes (Burre et al., 2014; Dettmer et al., 2016; 2017; Wang et al., 2014). The multimers cluster synaptic vesicles and regulate neurotransmitter release (Sun et al., 2019; Wang et al., 2014). Additionally, interactions between membrane lipids and α-Syn oligomers, which are believed to be the most toxic species of α-Syn, have been reported to be highly connected to the neurotoxicity induced by α-Syn oligomers (Alam et al., 2019; Fanning et al., 2020; Fusco et al., 2017; Musteikytė et al., 2021; Narayanan and Scarlata, 2001; Stckl et al., 2013). First and foremost, membrane permeabilization is considered to be the primary toxic mechanism of α-Syn oligomers (Danzer et al., 2007; Kim et al., 2009; Reynolds et al., 2011; Stckl et al., 2013; Stefanovic et al., 2015; Tsigelny et al., 2012; Volles et al., 2001). It has been demonstrated that α-Syn mutant oligomers also disrupt negatively charged lipid vesicles (Stefanovic et al., 2015; Tsigelny et al., 2012; Volles and Lansbury, 2002). After a study suggested that only oligomeric forms of the α-Syn mutant would have the ability to permeabilize anionic vesicles (Volles et al., 2001), other studies monitored the permeabilization of synthetic vesicles containing negatively charged lipids by A30P, E46K, and A53T oligomers using a fluorescence dequenching-based leakage assay (Agliardi et al., 2021; Volles and Lansbury, 2002). However, the effects of α-Syn mutant oligomers on synaptic vesicles, which have vesicular SNARE proteins, are largely unknown. As α-Syn mutant oligomers interact with synaptic vesicles in the brain, identifying what role they play in synaptic vesicles is a prerequisite for understanding the pathogenesis of α-Syn mutant oligomers.

Several studies have indicated that oligomeric forms of wild type (WT) α-Syn and their interactions with VAMP2 are the basis of synaptic dysfunction (Agliardi et al., 2021; Choi et al., 2013; 2018). WT α-Syn oligomers generated by dopamine bind directly to VAMP2 via their C-terminal domains and cluster VAMP2-associated vesicles, which results in inhibiting vesicle fusion (Choi et al., 2013; Yoo et al., 2021; 2022). Additionally, a post mortem study showed that more than 20% of the proteins found in Lewy bodies are SNARE proteins, including VAMP2 (McCormack et al., 2019). Recently, a correlation of high levels of α-Syn oligomers and low levels of free VAMP2 in peripheral neural extracellular vesicles with the severity of PD was reported (Agliardi et al., 2021), indicating the pathological role of the interactions between α-Syn oligomers and VAMP2. The interactions between the C-terminal region of α-Syn and VAMP2 are preserved in α-Syn mutants. However, whether those interactions exert aberrant effects on synaptic vesicles is still unknown.

In this study, we investigate the effect of α-Syn mutants associated with familial PD on SNARE-embedded vesicles. We show that interactions of A30P and A53T with VAMP2 cause clustering of VAMP2-reconstituted vesicles and subsequently inhibit vesicle fusion. On the other hand, E46K permeabilizes VAMP2-embedded lipid membranes in the presence of VAMP2 and anionic lipids. In the absence of interactions with VAMP2, E46K enlarges vesicles. Thus, we suggest a possible explanation for understanding the relationship between α-Syn mutant linked to PD and the clinical phenotypes of PD.

MATERIALS AND METHODS

Preparation and purification of WT and mutant α-Syn

Recombinant glutathione-S-transferase (GST)-tagged α-Syn was cloned into a pGEX-KG vector. A53T, A30P, and E46K α-Syn mutant constructs were generated by oligonucleotide site-directed mutagenesis of the WT construct. WT and mutant α-Syn constructs were transformed into *Escherichia coli* BL21 Rosetta (DE3) pLysS (Novagen, Germany). The purification procedures of α-Syn have been described elsewhere (Yoo et al., 2021). Briefly, cells were grown at 37°C in Luria–Bertani (LB) medium with 100 μg/ml ampicillin and induced by the addition of 0.5 mM isopropyl β-d-thiogalactopyranoside overnight at 16°C. Pelleted cells were resuspended in lysis buffer (1% sarcosine and 2 mM 4-(2-aminoethyl) benzenesulfonyl fluoride hydrochloride in 1× phosphate-buffered saline [PBS] buffer). After sonication of the cells, glutathione-agarose beads were used for affinity chromatography, and α-Syn protein was cleaved from a resin by a thrombin (30 U) reaction. Proteolysis was stopped by addition of 4-(2-aminoethyl)-benzenesulfonyl fluoride hydrochloride (AEBSF) to a final concentration of 1 mM.

Preparation of α-Syn oligomeric mixtures and purified oligomers

Oligomeric mixtures were prepared by incubating 0.5 mg/ml (i.e., 33 μM) of recombinant α-Syn mutant monomers in PBS 1X buffer (pH 7.4) with agitation at 37°C. The aggregation status of the protein mixtures was monitored daily using thioflavin T (ThT) fluorescence assays and TEM. The oligomeric mixtures after incubation for three days were used for experiments. To separate α-Syn mutant oligomers from monomers, size exclusion chromatography was performed using Superdex 200 increase 10/300 GL (GE Healthcare, USA). Then, the eluates were collected and concentrated by ultrafiltration with MWCO 10 kDa filter (Millipore, USA). Dopamine-induced α-Syn oligomers were prepared by incubating 15 μM of WT α-Syn with 100 μM dopamine in 20 mM sodium phosphate buffer (pH 7) at 37°C for 72 h. After incubation, dopamine-induced α-Syn oligomers were purified similarly to α-Syn mutant oligomers. The purified α-Syn oligomers are typically stable for weeks when they are split to aliquots, snap-frozen and stored at –80°C until further use (Kumar et al., 2020).

Transmission electron microscopy (TEM)

A 200-mesh carbon grid (Electron Microscopy Sciences, USA) was glow-discharged using the PELCO easiGlow plasma cleaning system (Ted Pella Inc., USA). A droplet of sample solution (3 μl) was placed on a grid for 30 s and removed using filter paper. Next, 2% uranyl acetate was used for negative staining. The grid was left to air dry before imaging. A

transmission electron microscope (FEI Talos L120C; Thermo Fisher Scientific, USA) was used to detect α-Syn aggregates, operating at a 120-kV acceleration voltage in the Nanobioimaging center of Seoul National University.

Preparation and purification of SNARE proteins
His6×-tagged syntaxin HT (amino acids 168-288; two cysteines replaced with alanines) was inserted into the pET28a vector and purified using a Ni-NTA resin column. GST-tagged synaptosomal-associated protein 25 (SNAP-25) (amino acids 1-206; four cysteines replaced with alanines), VAMP2 (amino acids 1-116; one cysteine was replaced with alanine), and an N-terminal truncated mutant of VAMP2 (nt-VAMP2, amino acids 29-116) were inserted into the pGEX-KG vector and purified by a glutathione-agarose resin column. BL21 Rosetta (DE3) pLysS (Novagene) cells were used for the expression of all proteins.

Protein concentration calculation
The concentrations of α-Syn mutant monomers were measured by absorption measurements with a NanoDrop spectrophotometer (Thermo Fisher Scientific), using a theoretical extinction coefficient of 5,960 M^{-1} cm^{-1}. The concentrations of α-Syn mutant oligomers were determined by DC protein assay (Bio-Rad, USA) with bovine serum albumin as a standard. The concentration values given in this work represent the total mass concentration of protein.

Preparation of small unilamellar vesicles (SUV)
Synthetic lipid components, including 1-palmitoyl-2-oleoyl-sn-glycero-3-phosphocholine (POPC), 1,2-dioleoyl-sn-glycero3-(phospho-L-serine) (DOPS), cholesterol (Chol), 1,2-dioleoyl-sn-glycero-3-phosphoethanolamine-N-[methoxy(polyethylene glycol)-5000] (PEG-PE), and 1,2-dipalmitoyl-sn-glycero-3-phosphoethanolamine-N-(lissamine rhodamine B sulfonyl) (Rhod-PE), were purchased from Avanti Polar Lipids (USA). As indicators in the lipid mixing assay, the lipid analog fluorescent dyes DiI and DiD were used as FRET donor and acceptor dyes, respectively (Invitrogen, USA). Chloroform stock solutions were mixed, and the chloroform was removed under vacuum in a desiccator for 16 h. The molar ratio of POPC:DOPS:PEG-PE was 92:7:1, and 10^{-5} mol % Rhod-PE was added for the formation of the supported lipid bilayer (SLB). For an *in vitro* lipid mixing assay, the molar ratio of POPC:DOPS:Chol:DiI (or DiD) was 71:7:20:2. The lipid mixtures were then rehydrated in 25 mM HEPES buffer with 100 mM KCl (pH 7.4), and ten freeze-and-thaw cycles were performed using liquid nitrogen and a water bath at 37°C. The solution was passed through a mini extruder (Avanti Polar Lipids) ten times with a 100 nm polycarbonate filter (Whatman, UK). Next, extrusion was performed to obtain monodisperse unilamellar vesicles using a mini extruder (Avanti Polar Lipids) with a 100 nm polycarbonate filter (Whatman).

Reconstitution of proteoliposomes
Incorporation of membrane proteins into the vesicles was achieved by diluting a detergent-solubilized protein/vesicle mixture and reducing the concentration of the detergent below the critical micelle concentration (CMC). We used the detergent n-octyl-β-D-glucopyranoside (OG) (Sigma, USA). For the formation of SLBs, VAMP2-to-lipid ratios were 1:500. In contrast, the protein-to-lipid ratios were 1:200 for an *in vitro* lipid mixing assay. To form pre-t-SNARE complexes, syntaxin HT and SNAP-25 (molar ratio of 1:2) were incubated with agitation for 1 h at room temperature for preventing the formation of dead-end t-SNARE complexes. DiI-labeled vesicles were then mixed with pre-t-SNARE complexes and OG to form t-vesicles with agitation for 30 min at 4°C. VAMP2 was added to DiD-labeled vesicles with OG to form v-vesicles with agitation for 30 min at 4°C. Two different vesicles were rapidly diluted in 25 mM HEPES buffer with 100 mM KCl (pH 7.4) to reduce the concentration of OG below its CMC.

Formation of SLBs
Glass coverslips (22 mm × 22 mm) were washed in 1 M KOH solution with sonication for 10 min. After rinsing with purified water, coverslips were used immediately after cleaning. SUV solutions were spread onto the coverslip surface and incubated for 30 min at 37°C. After that, nonadsorbed vesicles were removed by changing the buffer.

Fluorescence microscopy and imaging acquisition
A home-built objective-type total internal reflection fluorescence microscope (TIRFM) based on a Nikon Eclipse Ti-E inverted microscope was used for fluorescence imaging. A shutter-controlled 532 nm laser of 5-10 W/cm^2 intensity (for Rhod-PE, Cobolt Dual Calypso, Cobolt) was collimated to focus on the back focal plane of an oil-immersion objective lens (CFI Apo TIRF 100×, numerical aperture 1.49). A 1.5× amplifier was used to achieve 150× magnification. The emission light passed through a dichroic mirror (ZT532/640rpc; Chroma, Taiwan) and emission filters (ET590/50m; Chroma) and was collected by an electron multiplying charge-coupled device (EM-CCD) camera (iXon Ultra 888; Andor Technology, UK). The measurement of imaging was controlled by Metamorph Software, and maintaining focus during data acquisition was achieved using a Perfect Focus System.

Single-particle tracking
Single-particle tracking was analyzed using a home-built algorithm in MATLAB that originated from the u-track program (Jaqaman et al., 2008). The distribution of the diffusion coefficients was acquired by calculating each trajectory from the mean square displacement (MSD) to measure the diffusion coefficient using the two-dimensional free diffusion model equation. Only the single spot of molecule with threshold of SNR 3 and duration 5 frames was used for analysis. For each data, more than 10,000 trajectories were analyzed. Each time point of the image was taken in a stream of 200 frames with a frame rate of 50 ms. The detailed procedures have been described elsewhere (Cho et al., 2021).

In vitro lipid mixing assay
t-Vesicles and v-vesicles were mixed together to reach a 20 μM lipid concentration with or without α-Syn variants at 37°C. The final reaction volume was 60 μl. We induced excitation of the DiI-doped t-vesicles using 532-nm light and detected the FRET signal (at 690 nm) every 10 s for 2,000 s

using a temperature-controlled fluorescence spectrophotometer (Cary Eclipse; Agilent, USA).

Cryo-electron microscopy (cryo-EM)
Vesicles were incubated without or with α-Syn variants for 10 min. The molar ratio of lipids to the α-Syn mutants (in monomeric units) was 250:1. A 200-mesh carbon grid (Electron Microscopy Sciences) was glow-discharged using the PELCO easiGlow plasma cleaning system (Ted Pella Inc.). Sample vitrification was performed using a vitrification robot (FEI, Netherland) by plunging the samples in liquid ethane. After loading samples on the grids, they were automatically blotted with filter paper and plunge-frozen in liquid ethane. The grids were then mounted in dedicated cartridges and stored in liquid nitrogen until imaging. The vitrified specimens were examined using an FEI Talos L120C Cryo-EM instrument operating at a 120-kV acceleration voltage in the Nanobioimaging center of Seoul National University.

Preparation of sulforhodamine B (SRB)-filled vesicles and SRB dequenching assay
SRB (20 mM) were added to the lipid mixture during rehydration. The extrusion and protein reconstitution procedures were identical to those of proteoliposomes doped with DiI or DiD. After the recovery of samples from a dialysis tube, free SRB dyes were removed by a Sepharose CL-4B resin column (Sigma). We incubated the vesicles with E46K oligomers for 10 min and then performed an SRB dequenching assay. When vesicles are intact and undamaged, self-quenching between SRB molecules occurs, which reduces the fluorescence intensity of SRB. When SRB is released to solution by vesicle disruption, the SRB concentration decreases and thus self-quenching does not occur. As a result, the fluorescence intensity of SRB increases by the vesicle disruption. We used 532-nm light for excitation and monitored SRB dequenching at 580 nm every 10 s using a temperature-controlled fluorescence spectrophotometer (Cary Eclipse).

Data analysis to quantify the extent of vesicle remodeling by E46K oligomers
The eccentricity and circularity of each vesicle visualized by cryo-EM were measured on 332 randomly selected vesicles. Analysis was performed using a custom-built program (MATLAB 2017b, MathWorks).

Dynamic light scattering
The size of the vesicles was measured using a Zetasizer (Zetasizer Nano ZSP; Malvern Instruments, UK) at 25°C. The sample was placed inside the Zetasizer, and the intensity of the laser light scattered by the sample preparations was measured at 90° to the incident light. The data were analyzed using Malvern software supplied with the machine, and the size distribution and the Z-average diameter were obtained.

RESULTS

A30P, E46K, and A53T oligomers were generated by incubating recombinant monomers
Normally α-Syn is an intrinsically disordered monomeric protein that is quite stable (Eliezer, 2009). To induce its aggregation, exposure to pesticides, heavy metals, dopamine, chemical crosslinking reagents and excess amounts of α-Syn protein are required (Conway et al., 2001; Danzer et al., 2007; Kumar et al., 2020). However, three missense mutations in α-Syn were found to accelerate the conversion of monomers to oligomers (Conway et al., 1998; 2000; Danzer et al., 2007; Lashuel et al., 2002; Li et al., 2001). Thus, we asked whether α-Syn mutant monomers in physiological concentrations would generate oligomeric species without any additive. In previous studies, α-Syn was estimated to be present at 30-60 μM in presynaptic boutons (Bodner et al., 2009; Iwai et al., 1995). Thus, 0.5 μg/ml (i.e., 33 μM) of recombinant α-Syn monomers were incubated with agitation at 37°C (Figs. 1A and 1B). Then, we monitored the aggregation status of protein samples daily using ThT fluorescence assays until α-Syn eventually self-assembled into fibrils (Fig. 1C). Among the α-Syn variants, E46K exhibited the most rapid conversion into fibrils (Fig. 1C), which was detected by TEM (Supplementary Fig. S1). After incubation with agitation for 3 days, α-Syn protein mixtures were assessed by TEM (Fig. 1D). As shown in Fig. 1D, A30P, A53T, and E46K generated various sizes of oligomers, while WT α-Syn did not assemble into any detectable structure (Fig. 1D). α-Syn fibrils were not detected in any sample (Fig. 1D). In our experimental conditions, all types of α-Syn converted to fibrils within the timespan of several days. After 3 days of incubation, however, the major populations of α-Syn mutants were oligomeric forms prior to fibril assembly. Using size exclusion chromatography, we measured the fraction of oligomers to ensure that each reaction was reproducible (Supplementary Table S1, Supplementary Fig. S2). The fractions of oligomers of A30P, A53T, and E46K in our sample preparation were calculated as 71.6% ± 2.1%, 87.8% ± 0.8%, and 92.1% ± 0.5% (n = 5, SEM), respectively. E46K and A53T generated larger sizes of oligomers than A30P (Supplementary Fig. S2-S4). Since the major species in the reaction mixtures were oligomers and multiple routine processing steps for oligomer purification can alter protein aggregation (Wang, 2005; Wang et al., 2010), we used the whole mixture of α-Syn mutant solution after incubation for 3 days. We also used the purified α-Syn mutant oligomers to confirm the effects of α-Syn oligomers in the mixture.

E46K oligomers reduce the lateral mobility of the membrane lipid in VAMP2-embedded SLB
We first tested whether α-Syn mutant oligomers change membrane mobility by permeabilizing or disrupting the VAMP2-embedded lipid membranes. Disruption or alteration in membrane structure can affect membrane mobility, which is a critical parameter for physiological functions of the membrane, such as vesicle trafficking and signal transduction (Jacobson et al., 2019; van Meer et al., 2008). Although many studies have observed the release of fluorescent dye encapsulated in vesicles after the addition of α-Syn mutant oligomers, no study has investigated alterations in membrane mobility resulting from membrane disruption. Thus, we prepared a PEG-tethered SLB, a stable planar membrane platform, to collect data on membrane mobility (Jackman and Cho, 2020; Richter et al., 2006).
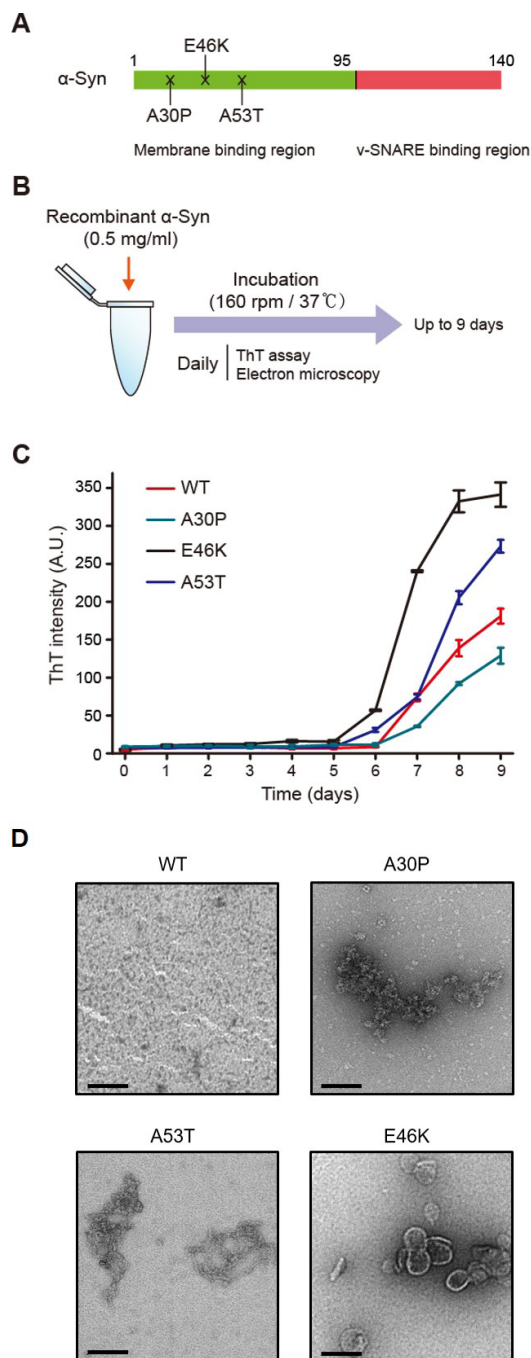
A

B

C

D

Fig. 1. *In vitro* generation of A30P, A53T, and E46K oligomers. (A) Schematic representation of α-Syn domains. Missense mutations known to cause familial PD (A30P, A53T, and E46K) lie in the amphipathic region (light green), responsible for binding to anionic membrane lipids. The acidic C-terminal region from amino acids 96-140 (red) interacts with VAMP2. (B) Generation of oligomers comprising WT, A30P, E46K, or A53T α-Syn. α-Syn (0.5 μg/ml) in 1X PBS buffer (pH 7.4) was incubated at 37°C with continuous shaking. (C) The change in fluorescent intensity of ThT (λex/em = 450/480 nm) during α-Syn variant fibrilization (n = 3, ± SEM). (D) TEM images of α-Syn samples after 3 days of incubation. No aggregates were observed in WT α-Syn, while A30P, A53T, or E46K oligomers were detected. Scale bars = 100 nm.

SLBs were prepared on clean hydrophilic glass surfaces by spreading SUV reconstituted with VAMP2 (Fig. 2A). We included 10^{-5} mol % rhodamine-PE (Rhod-PE) to trace the diffusion of lipids using single particle tracking (Cho et al., 2021) and 7 mol % DOPS, the negatively charged phospholipid. Before the addition of α-Syn oligomeric mixtures, we confirmed the overall quality of the SLBs by testing whether the bilayer was continuous and that lipid molecules were laterally mobile (see Supplementary Movie S1). The diffusion coefficient of Rhod-PE was constant for at least 30 min after the formation of SLB (Supplementary Fig. S5).

Having established that the SLB was well formed, we then added mutant oligomeric mixtures (75 nM in total monomer concentration) and dopamine-induced α-Syn WT oligomers to SLBs. Since α-Syn WT monomers did not generate oligomers after 3-day agitation (Fig. 1D), we used dopamine-induced α-Syn WT oligomers for the comparison. Dopamine-induced α-Syn WT oligomers are kinetically stabilized non-amyloidogenic oligomers (Choi et al., 2013; Conway et al., 2001; Yoo et al., 2021).

To quantitatively analyze changes in membrane mobility in response to α-Syn mutant oligomeric mixtures, we measured the diffusion coefficient (D) of Rhod-PE before and 30 min after treatment with α-Syn mutant oligomeric mixtures. The change in mobility of Rhod-PE was indicated by the diffusion coefficient shift, which was calculated as follows: diffusion coefficient shift (%) = 100 $[(D_{30\ min\ after\ treatment} - D_{before\ treatment})/D_{before\ treatment}]$ (Kim et al., 2015). A diffusion coefficient shift lower than zero indicates the reduced mobility of Rhod-PE. After incubation for 30 min, we observed that Rhod-PE was laterally mobile even after the treatment with dopamine-induced α-Syn WT oligomers (Figs. 2B, 2C, and 2F). However, E46K oligomeric mixture (75 nM in total monomer concentration) significantly decreased the mobility of Rhod-PE (Figs. 2D, 2E, and 2G, Supplementary Fig. S6; see also Supplementary Movie S2). The diffusion coefficient shift in the Rhod-PE diffusional mobility by E46K oligomeric mixture was approximately −90% (Fig. 2H). Additionally, there was no detectable change in the diffusivity of Rhod-PE after incubation with the E46K monomer, implying that the decrease in lipid diffusional mobility induced by E46K was specific to the presence of E46K oligomers (Supplementary Fig. S7). Indeed, we confirmed that purified E46K oligomers also decreased the mobility of the membrane lipids (Supplementary Fig. S8).

In contrast, A30P and A53T oligomeric mixtures did not change the mobility of the lipid (Fig. 2H, Supplementary Fig. S9). These results were also confirmed using purified A30P and A53T oligomers (Supplementary Fig. S8). Again, the monomers of WT α-Syn, A30P, and A53T had no effect on the mobility of the lipid (Supplementary Fig. S7). A30P oligomers are known to exhibit reduced membrane binding affinity compared to WT, while A53T oligomers bind to the membrane with a similar affinity as WT (Giannakis et al., 2008). Regardless of membrane binding affinity, neither A30P or A53T oligomeric mixtures affected membrane mobility, implying that membrane binding of these α-Syn mutants may not be sufficient for their ability to immobilize membrane lipids.
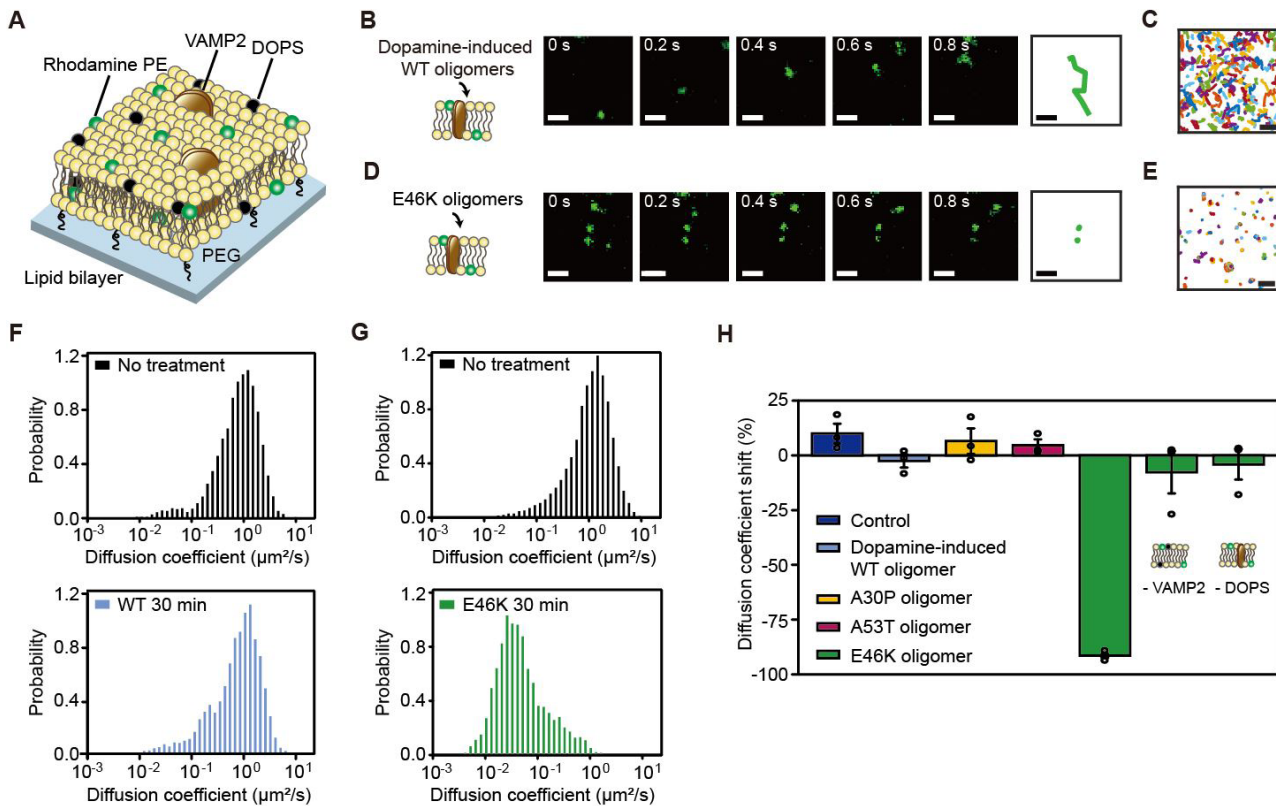
Next, we examined whether the presence of VAMP2 was

Fig. 2. Alterations in membrane lipid mobility by treatment with α-Syn variant oligomers. (A) Schematic illustration of the experimental design to measure the mobility of the membrane in the presence of VAMP2. The fluorescent probe Rhod-PE was used to detect the diffusion of membrane lipids in the SLBs. Fluorescence images (50 ms/frame) were obtained by an objective-type total internal reflection fluorescence microscope. Each trajectory of a lipid was analyzed by a home-built algorithm based on the u-track program and then the diffusion coefficient of each trajectory was calculated from the mean square displacement with the two dimensional free diffusion model. (B) Time-lapse images are presented with 0.2 s intervals, which show the movement of the fluorescent membrane lipid molecule after the addition of dopamine-induced α-Syn WT oligomers. The right panel shows maps of accumulated trajectories of individual lipid molecule acquired for about 0.8 s after the treatment of dopamine-induced α-Syn WT oligomers. Scale bars = 1 μm. (C) Trajectory maps of lipids after the treatment with dopamine-induced α-Syn WT oligomers (after 30 min) in the SLBs. Randomly chosen trajectories acquired for approximately 2 s are shown. Scale bar = 1 μm. (D) Time-lapse images are presented with 0.2 s intervals, which show the movement of the fluorescent membrane lipid molecule after the addition of α-Syn E46K oligomeric mixtures. Scale bars = 1 μm. (E) Trajectory maps of lipids after the treatment with α-Syn E46K oligomeric mixtures (after 30 min) in the SLBs. Randomly chosen trajectories acquired for approximately 2 s are shown. Scale bar = 1 μm. (F) Diffusion coefficient distributions of Rhod-PE trajectories on a logarithmic scale before (no treatment, black) and 30 min after treatment with dopamine-induced α-Syn oligomers (WT 30 min, light blue). (G) Diffusion coefficient distributions of Rhod-PE trajectories on a logarithmic scale before (no treatment, black) after 30-min incubation with E46K oligomeric mixtures (E46K 30 min, green). Sum of the probability was normalized to 1. (H) Mean diffusion coefficient of the Rhod-PE in the VAMP2 embedded SLBs containing negatively charged lipid DOPS was measured before and after the treatment with α-Syn mutant oligomeric mixtures (control: PBS buffer treatment). Only E46K oligomeric mixtures immobilized membrane lipid (green bar). In the absence of VAMP2 (-VAMP2) or DOPS (-DOPS), however, the mobility of membrane lipids was not reduced by E46K oligomers. The error bars indicate the mean ± SEM of three independent measurements.

responsible for membrane immobilization by E46K oligomeric mixtures. We prepared SLBs without VAMP2. In the SLBs without VAMP2, E46K oligomeric mixture did not affect lipid mobility (Fig. 2H, -VAMP2 and Supplementary Fig. S9). Also, E46K oligomeric mixture did not change the diffusivity of the membrane in neutral SLBs (Fig. 2H, -DOPS and Supplementary Fig. S9). We repeated these experiments with purified E46K oligomers, and observed the same results (Supplementary Fig. S8). Therefore, we concluded that E46K oligomers

immobilize the membrane lipids in the presence of VAMP2 and anionic lipids.

A30P and A53T oligomers inhibit SNARE-mediated lipid mixing

E46K oligomers damaged the mobility of VAMP2-carrying membrane lipids, but A30P and A53T oligomers did not affect it (Fig. 2H, Supplementary Fig. S8). Thus, we examined the effect of the interactions of A30P and A53T oligomeric

mixtures with VAMP2 on SNARE-driven membrane fusion.

We prepared two different proteoliposomes labeled with two different fluorescence dyes for an *in vitro* lipid mixing assay (Choi et al., 2013; Kim et al., 2012; Yoo et al., 2021). We incorporated t-SNAREs (complexes of syntaxin HT [amino acids 168-288 of syntaxin 1A, lacking the Habc domain] and SNAP25) and VAMP2 into t- and v-vesicles, respectively. For SNAP25, four native cysteine residues were replaced with alanine. When t-vesicles doped with DiI (T) and v-vesicles doped with DiD (V) were fused together through SNARE complex formation, lipid mixing between the two types of vesicles occurred. This lipid mixing was monitored by the fluorescence resonance energy transfer (FRET) signal between DiI and DiD (Fig. 3A) (Yeou and Lee, 2022). Significant lipid mixing was detected in the T-V mixture (Figs. 3B and 3C, black line). We confirmed that lipid mixing was caused by SNARE complex formation by observing that the addition of the soluble domain of VAMP2 (solVP) did not result in any increase in the FRET signal (Figs. 3B and 3C, gray line). WT α-Syn oligomers generated by dopamine are known to interfere with SNARE-mediated lipid mixing (Choi et al., 2013; Yoo et al., 2021). We tested whether α-Syn mutants' oligomeric mixtures also affect SNARE-mediated lipid mixing. As a result,

inhibitory effects on lipid mixing were observed from 200 to 850 nM of A30P or A53T samples (in total monomer concentration) (Figs. 3B and 3C). In contrast, WT α-Syn samples under the same incubation conditions without dopamine, where oligomeric forms were not detected by TEM (Fig. 1D), had a negligible effect on vesicle fusion (Supplementary Fig. S10). We also assessed the effect of A53T or A30P monomer at the same concentrations without incubation, which produced no effects on vesicle fusion (Supplementary Fig. S11). Thus, this inhibitory effect of PD-linked mutants is dependent on the presence of oligomeric species. The same results were observed when we repeated these experiments using purified A30P and A53T oligomers (Supplementary Fig. S12).

We then investigated the mechanism underlying fusion inhibition by A30P and A53T oligomers. We previously reported that WT α-Syn oligomers generated by dopamine block SNARE-mediated vesicle fusion via interactions with the N-terminus of VAMP2 (Choi et al., 2013). Thus, we suspected that A30P and A53T oligomers also interacted with the N-terminal domain of VAMP2, which may have resulted in inhibitory effects on fusion. To test this hypothesis, we prepared an N-terminal truncated VAMP2 (amino acids 29-116) (Fig. 3D). We then added A30P and A53T oligomeric mix-
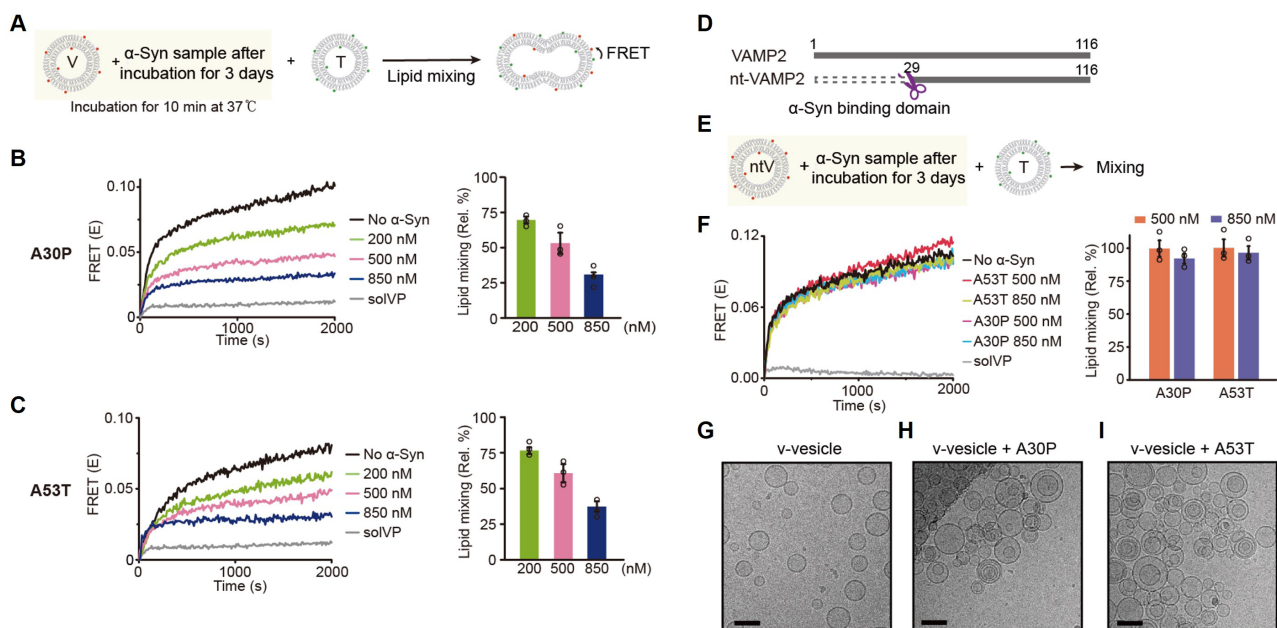

Fig. 3. Effects of A30P and A53T oligomers on SNARE-mediated lipid mixing. (A) A scheme of *in vitro* lipid mixing assays. The results of lipid mixing between t-vesicles and v-vesicles after the treatment of α-Syn protein samples after 3-day incubation are shown in (B) A30P and (C) A53T. While WT α-Syn sample after 3 days of incubation had a negligible effect on SNARE-mediated lipid mixing, A53T and A30P samples prepared under the same conditions inhibited vesicle fusion. More severe inhibition of vesicle fusion between T and V was observed as the concentration of α-Syn increased. Lipid mixing was confirmed to be driven by SNARE complex formation by the addition of the soluble domain of VAMP2 (solVP), which blocked lipid mixing. Bar graphs were obtained from relative percentages (Rel. %) of lipid mixing at 2,000 s (± SEM, n = 3). (D) N-terminal truncated VAMP2 was prepared. (E) Scheme of testing the effect of α-Syn mutant oligomeric mixtures on the fusion reaction with v-vesicles reconstituted with N-terminal truncated VAMP2 (ntV). (F) The inhibitory effect of A30P and A53T protein samples after 3 days of incubation on lipid mixing was not observed in the absence of VAMP2. Relative percentages of fusion between the two types of vesicles at 2,000 s from the FRET data are summarized in the bar graph (± SEM, n = 3). Representative image of (G) v-vesicles in the absence of α-Syn mutant oligomeric mixtures, (H) v-vesicles with A30P oligomeric mixtures, and (I) v-vesicles with A53T oligomeric mixtures. Scale bars = 100 nm.

tures to the vesicles reconstituted with N-terminal truncated VAMP2 (ntV) and incubated the mixture for 10 min (Fig. 3E). Next, we added T to the premixture and monitored the FRET signal (Fig. 3E). As a result, A30P and A53T oligomeric mixtures did not have any significant inhibitory effect on lipid mixing between T and ntV (Fig. 3F), demonstrating that the presence of the N-terminal domain of VAMP2 is required for the fusion inhibitory effect of the mutants.

A30P and A53T oligomers cluster VAMP2-embedded vesicles

Next, we investigated how A30P and A53T oligomers block SNARE-mediated lipid mixing. In our previous studies, we showed that WT α-Syn oligomers generated by dopamine cluster VAMP2-embedded vesicles and inhibit subsequent vesicle fusion (Choi et al., 2013; Yoo et al., 2021). Therefore, we speculated that the fusion inhibition effect of A30P and A53T oligomers might also result from their activity to cluster VAMP2-embedded vesicles. To confirm this, we used cryo-electron microscopy (cryo-EM) to directly visualize the morphology of vesicles. In the absence of α-Syn oligomeric mixture, VAMP2-carrying vesicles (v-vesicles) were separated from each other (Fig. 3G). However, after the addition of either A30P or A53T oligomeric mixture, v-vesicles clustered together (Figs. 3H and 3I, Supplementary Fig. S13), which is consistent with our previous findings by dopamine-induced WT α-Syn oligomers (Yoo et al., 2021). In this work, monomeric A30P or A53T sample without incubation did not induce v-vesicle clustering (Supplementary Fig. S14). This result seems to be different from the previous study, which showed that α-Syn monomer induces vesicle clustering (Diao et al., 2013). The clustering by α-Syn monomer occurs at the micromolar α-Syn concentration and higher protein-to-lipid ratios (Diao et al., 2013). However, in this work we used sub-micromolar concentration, at which no inhibition of vesicle fusion was observed before (DeWitt and Rhoades, 2013). Taken together, clustering of VAMP2-embedded vesicles is a shared aberrant mechanism among dopamine-induced WT α-Syn, A30P, and A53T oligomers, which may lead to interference with SNARE-dependent vesicle fusion. Additionally, interac-
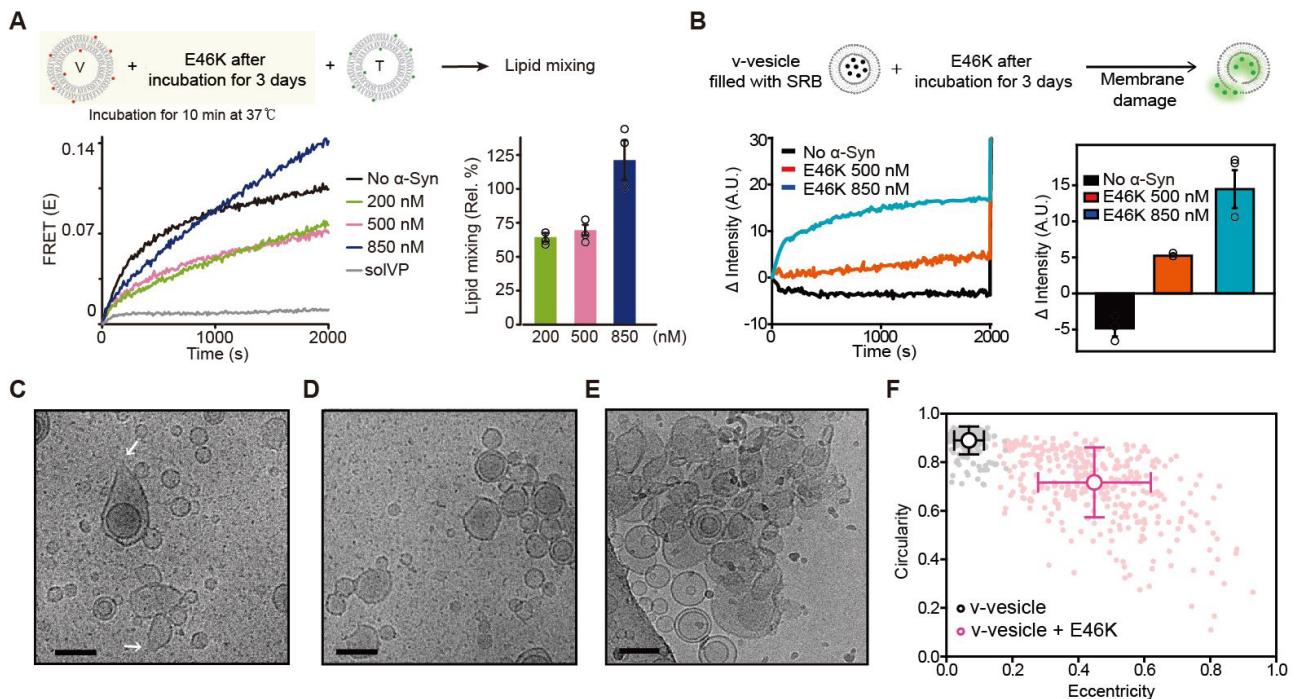

Fig. 4. The membrane permeabilizing effect of E46K oligomers by interacting with VAMP2. (A) FRET signals from the mixture of T and V after the addition of E46K oligomeric mixtures. Lipid mixing was confirmed to be driven by SNARE complex formation by the addition of the soluble domain of VAMP2 (solVP), which blocked lipid mixing. The results from three independent measurements are summarized in the bar graph (± SEM). Rel. %, relative percentages. (B) Results of vesicle leakage assays. SRB (20 mM) was encapsulated in v-vesicles in a fluorescently quenched state. Without α-Syn samples, no disruption of the vesicles was observed, and the fluorescence intensity of SRB decreased for 2,000 s at 37°C due to SRB bleaching (black line). After the addition of α-Syn E46K oligomeric mixtures, the fluorescence intensity of SRB increased due to membrane permeabilization. After 2,000 s, 0.5% Triton X-100 was added to the reaction mixture to solubilize the vesicles and verify the encapsulation of SRB. The results of SRB measurement are summarized in the bar graph (± SEM, n = 3). (C-E) Representative images of v-vesicles after the addition of E46K oligomeric mixtures detected by cryo-EM. E46K oligomeric mixtures deformed and perforated vesicles. (C) The pores on the membrane (white arrows), (D) elongated vesicles into a row of sausage-like shapes, and (E) crushed vesicles were visualized. Scale bars = 100 nm. (F) The variation in circularity and eccentricity of vesicles in response to E46K sample is visualized in scatter plots. For v-vesicles, most of the data congregate in the upper-left corner, suggesting that the vesicles were round. In contrast, the data from the vesicles with α-Syn E46K sample are widely scattered, indicating that they were elliptical.

tions of α-Syn variant oligomers with VAMP2 are essential for this mechanism.

E46K oligomers permeabilize VAMP2-embedded vesicles

We observed that E46K oligomers significantly reduced the membrane mobility of the SLBs in the presence of VAMP2 and anionic lipids, while A30P or A53T oligomers had no effect (Fig. 2H, Supplementary Fig. S8). Thus, we speculated that E46K oligomers would have a distinct effect on VAMP2-embedded vesicles than A30P and A53T oligomers, which cluster VAMP2-embedded vesicles. We first performed a lipid mixing assay in the presence of E46K oligomers. The FRET signal was not saturated and increased sharply after treatment with 850 nM E46K oligomeric mixtures (in total monomer concentration) (Fig. 4A). The purified E46K oligomers also showed the same effect on vesicle fusion (Supplementary Fig. S12). Such increases in FRET may reflect the occurrence of energy transfer caused by vesicle disruption rather than the kinetics of vesicle fusion.

Thus, to confirm the ability of E46K oligomers to disrupt VAMP2-embedded vesicles, we tested whether the fluorescent dye encapsulated within the v-vesicle was released in response to treatment with E46K oligomeric mixtures. We prepared v-vesicles filled with SRB. The increase in the fluorescence intensity by SRB dequenching was used as an indicator of membrane permeabilization by E46K oligomeric mixtures in this assay (Fig. 4B). At appropriate time points after 2,000 s, 0.5% Triton X-100 was added to the reaction mixture to obtain a fluorescence signal at 100% SRB dequenching to verify encapsulation of SRB (Fig. 4B). In the absence of E46K, the fluorescence intensity of SRB decreased slightly by photobleaching (Fig. 4B, black). After the addition of E46K oligomeric mixtures, we observed that the fluorescence intensity of SRB increased, indicating that E46K oligomeric mixtures actually permeabilize VAMP2-embedded vesicles (Fig. 4B, red and blue). Again, purified E46K oligomers also increased the fluorescence intensity of SRB, while other purified mutant oligomers did not (Supplementary Fig. S15). However, the changes in fluorescence intensities of SRB were not remarkable, suggesting that the vesicles had only a small leak.

Next, we visualized the morphology of VAMP2-associated vesicles in the presence of E46K oligomers using cryo-EM (Figs. 4C-4E). In the absence of E46K oligomers, v-vesicles were intact and exhibited a round shape (Fig. 3G). However, the E46K oligomeric mixtures deformed and perforated the v-vesicles, as shown in the images in Figs. 4C-4E. As a result of the formation of pores on the membrane, the shape of the vesicle looked like a deflated balloon. The pores of the membrane were detected (Fig. 4C, white arrows), and some v-vesicles were clustered and elongated into a row of sausage-like shapes after fusion with one another (Fig. 4D). In addition, some v-vesicles were crushed like burst balloons (Fig. 4E). These results were in contrast to the observations of v-vesicles treated with A30P or A53T oligomeric mixtures, which were intact and circular (Figs. 3H and 3I). To perform quantitative analysis, we calculated the eccentricity and circularity of the v-vesicles with and without E46K oligomeric mixtures. As shown in Fig. 4F, most of the data from v-vesicles congregated in the upper-left corner, suggesting that

they are round-shaped. In contrast, data from vesicles in the presence of E46K oligomers were widely scattered, indicating that the vesicles are not circular. However, E46K monomers did not affect v-vesicle shape (Supplementary Fig. S14), indicating that the vesicle permeabilizing activity of E46K is dependent on the presence of their oligomeric forms.

We then investigated whether E46K oligomers are also capable of permeabilizing vesicles reconstituted with N-terminal truncated VAMP2 (ntV). If the interactions between E46K oligomers and VAMP2 are responsible for membrane permeabilization, E46K oligomeric mixtures would not disrupt ntV. To test this hypothesis, we performed an SRB dequenching assay, and no leakage of SRB was observed in ntV treated with E46K oligomeric mixtures (Supplementary Fig. S16). Taken together, these findings reveal that the interactions between E46K oligomers and VAMP2 permeabilize membranes of VAMP2-embedded vesicles to cause leakage of the contents.

E46K oligomers enlarge vesicles by merging them with each other through interactions with the membranes

Interactions between E46K oligomers and VAMP2 cause vesicle permeabilization, perhaps reducing membrane mobility in the SLBs. What happens when E46K oligomers do not interact with VAMP2? To answer this question, we examined the effect of E46K oligomeric mixtures on lipid mixing between ntV, vesicles reconstituted with N-terminal truncated VAMP2 and T vesicles reconstituted with binary t-SNARE (Fig. 5A). As a result, E46K oligomeric mixtures inhibited lipid mixing between the two types of vesicles, indicating that such inhibition was caused by membrane binding of E46K oligomers (Fig. 5A).

To further investigate the question on the activity of E46K oligomers when they do not interact with VAMP2, we first observed the morphology of ntV and SNARE protein-free vesicles (F) treated with E46K oligomeric mixtures using cryo-EM (Fig. 5B, Supplementary Fig. S17). Most vesicles were intact (Fig. 5B, Supplementary Fig. S17), which was sharply in contrast to the full-length VAMP2 reconstituted vesicles with E46K oligomeric mixtures (Figs. 4C-4E). Additionally, extension of the outer membrane was visualized, forming enlarged vesicles containing several internal vesicles like shopping bags (Fig. 5B, left). Enlarged vesicles with diameter of around 400 nm were often visualized (Fig. 5B, right). Indeed, vesicle elongation was also observed in the v-vesicles with the E46K oligomeric mixtures (Fig. 4D), indicating that membrane binding of E46K oligomers caused elongation of vesicles.

Then, for quantitative analysis of the change in vesicular size resulting from vesicle elongation by E46K oligomers, we used dynamic light scattering. We prepared three types of vesicles: full-length VAMP2 reconstituted vesicles (V), N-terminal truncated VAMP2 reconstituted vesicles (ntV), and VAMP2-free vesicles (F). Each of them was incubated with and without E46K oligomeric mixtures at RT for 10 min. The average size and size distribution of V did not change after the addition of E46K oligomeric mixtures (Supplementary Fig. S18). In contrast, the average size of F and ntV increased from approximately 110 to 160 nm because minor peaks at approximately 600 nm and above 5 μm appeared, indicating
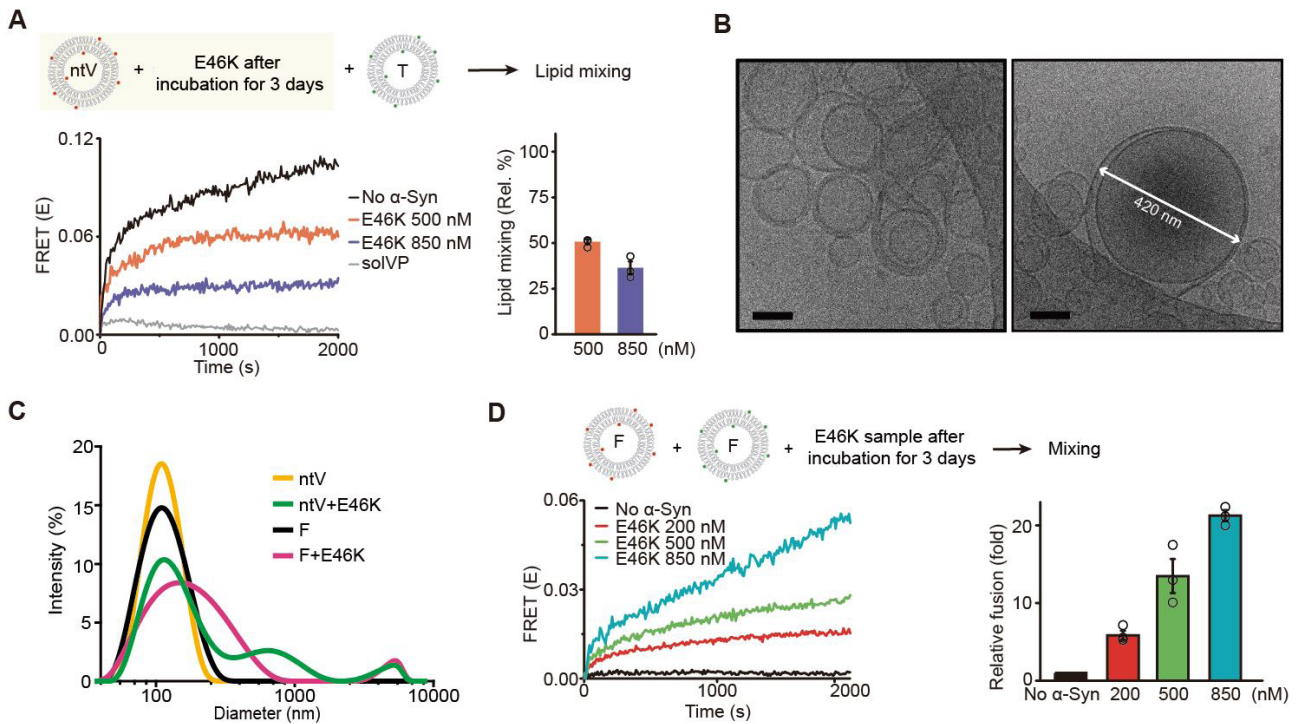
Fig. 5. VAMP2-independent vesicle enlargement by interactions of E46K oligomers with membrane lipids. (A) The inhibitory effect of E46K oligomeric mixtures on lipid mixing in the absence of VAMP2 (± SEM, n = 3). Lipid mixing was confirmed to be driven by SNARE complex formation by the addition of the soluble domain of VAMP2 (solVP), which blocked lipid mixing. (B) Representative images of enlarged ntV after the addition of E46K oligomeric mixtures detected by cryo-EM. Some of the vesicles were enlarged due to merging with one another, but the vesicles seem to be undamaged. An enlarged vesicle greater than 400 nm in diameter is visualized on the right panel. Scale bars = 100 nm. (C) Dynamic light scattering measurements of the two types of vesicles with and without E46K samples. The average size of the VAMP2-free vesicles (F) and the N-terminal truncated VAMP2 reconstituted vesicles (ntV) increased after mixing with E46K samples. (D) The results of SNARE-independent lipid mixing in response to treatment with E46K samples. Bar graphs were obtained from three independent measurements (± SEM, n = 3).

that E46K oligomeric mixtures induced vesicle elongation or aggregation (Fig. 5C).

To confirm that E46K oligomers enlarge vesicles by causing their fusion, which is distinct from SNARE-mediated vesicle fusion, we performed a lipid mixing assay using SNARE protein-free dye-labeled vesicles (Fig. 5D). The mixture of the two kinds of vesicles (vesicles doped with DiI and DiD) did not increase the FRET signal over time (Fig. 5D, black), indicating that lipid mixing between the vesicles is SNARE-dependent in this assay. After treatment with E46K oligomeric mixtures, surprisingly, the FRET signals increased over time (Fig. 5D), implying that E46K oligomers induce lipid mixing of vesicles. However, we cannot determine whether this lipid mixing was docking, lipid mixing, or content mixing between two vesicles using this assay. Taken together, these results revealed that E46K oligomers enlarged vesicles by interacting with membrane lipids in a SNARE-independent manner.

DISCUSSION

Familial PD induced by genetic mutations in α-Syn is rare, but analysis of its pathogenesis may substantially illustrate the mechanisms underlying the majority of sporadic PD. Howev-

er, differences in phenotypes according to the type of mutant imply that these pathogenic pathways are not straightforward (Petrucci et al., 2016; Tanaka et al., 2019). Although evidence is rare, specific genetic mutations were reported to lead to different phenotypes in the PD-dementia with Lewy bodies (DLB) spectrum. The A30P mutation is more often associated with classic PD, while the A53T mutant causes PD with multiple system atrophy (Petrucci et al., 2016; Tanaka et al., 2019). In addition, the E46K variant features rapidly developing DLB (Zarranz et al., 2004), which is similar to symptoms caused by triplications of the SNCA gene with short survival (Fuchs et al., 2007). The variation of phenotypes resulting from different mutants may be involved in the position of the mutation in the gene and its effects on protein function (Petrucci et al., 2016; Tanaka et al., 2019).

In this work, we focused on the toxic mechanisms of A30P, E46K and A53T mutant oligomers. α-Syn mutant oligomers were easily formed by incubating recombinant monomers at physiological concentrations for 3 days, while the WT α-Syn monomers remained in monomeric form (Figs. 6A and 6B). WT α-Syn and familial mutants commonly bind to VAMP2 and might proceed along the normal pathway, where α-Syn promotes SNARE complex formation (Fig. 6C), though the
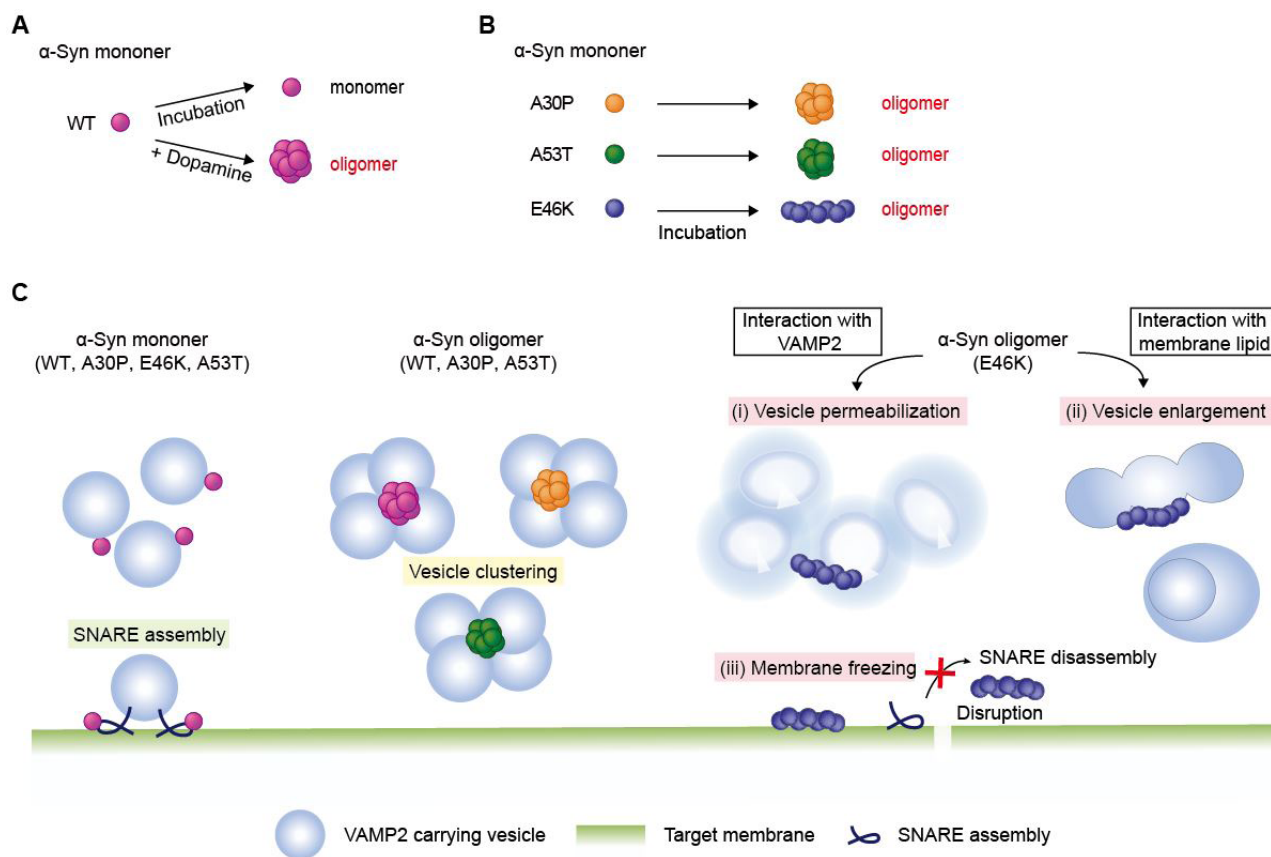
Fig. 6. The proposed mechanisms underlying dysfunctional synaptic vesicle fusion by oligomers of α-Syn mutants. (A) To generate oligomers of wild-type (WT) α-Syn, simple incubation of the monomer is not sufficient. Dopamine oxidation is one of the driving factors to oligomerize WT α-Syn. (B) Three α-Syn mutants, which have been identified as the cause for inherited PD, promote α-Syn protein oligomerization. 3-day incubation of recombinant monomer generates α-Syn mutant oligomers. (C) α-Syn monomers bind to VAMP2 and promote SNARE complex formation (left panel). A30P and A53T oligomers as well as WT α-Syn oligomers generated by dopamine oxidation induce vesicle clustering and inhibit vesicle fusion through their interactions with VAMP2 (middle panel). In contrast, E46K oligomers exert three effects on the membrane (right panel): (i) E46K oligomers permeabilize the VAMP2-embedded vesicles via binding to VAMP2, (ii) without interactions with VAMP2, E46K oligomers enlarge vesicles, (iii) E46K oligomers significantly reduce the membrane mobility and may penetrate presynaptic terminals.

physiological function of α-Syn to promote SNARE assembly is slightly decreased by A30P (Burre et al., 2012). In contrast, α-Syn oligomers comprising A30P or A53T inhibit SNARE-mediated vesicle fusion, which is a shared mechanism with WT α-Syn oligomers generated by dopamine oxidation (Fig. 6C). This abnormal action of α-Syn mutant oligomers can limit an available pool of synaptic vesicles and block neurotransmission. On the other hand, E46K oligomers have membrane remodeling abilities to permeabilize and enlarge vesicles by causing them to fuse with one another (Fig. 6C). This result may explain the previous findings that α-Syn oligomers were reported to rupture synaptic vesicles, prevent neurotransmitter release and impair intracellular Ca^{2+} homeostasis (Danzer et al., 2007; Furukawa et al., 2006; Tsigelny et al., 2012). They can also inhibit SNARE complex disassembly by immobilizing the membrane (Fig. 6C) and disrupting the presynaptic membrane. The membrane permeabilizing activity of E46K oligomers may accelerate the transmission of E46K oligomers to other parts of the brain, causing the extensive burden of

Lewy bodies.

However, the limitation of this *in vitro* study is that α-Syn oligomers generated *in vitro* could have different compositions, sizes, and shapes of those found in the brains of patients with PD. We note that this work is also limited to oligomeric species composed of α-Syn mutants created by incubation for 3 days with agitation; there are several methods to generate α-Syn oligomers, and different types of oligomers prepared using different protocols have been shown to exert different toxic effects, despite being the same mutation (Danzer et al., 2007; Kumar et al., 2020; Pieri et al., 2016). Previously, oligomers of A53T, A30P, or E46K were reported to permeabilize membrane lipids by binding to membranes (Stefanovic et al., 2015; Tsigelny et al., 2012; Volles and Lansbury, 2002). However, in our experiments, only E46K oligomers possessed a membrane permeabilizing function, which was attributed to interactions with VAMP2 and membrane lipids. Whether and how the α-Syn mutant oligomers we used in the present work differ structurally from those in pre-

vious studies is not known. One study prepared three types of α-Syn oligomers using different protocols and found that these different oligomer types led to cellular damage through distinct mechanisms (Danzer et al., 2007). In addition to differences in the aggregation methods, the lipid composition and the incorporation of VAMP2 in the vesicles might explain this discrepancy.

Additionally, we note that the protein samples we used were a mixture of heterogeneous forms of α-Syn, including oligomeric species, the distribution of which depends on the mutation. 0.5 mg/ml (33 μM) of α-Syn WT monomers did not form detectable oligomeric species as determined by TEM after 3 days of incubation. Under the same conditions, however, the α-Syn mutation itself caused a monomer-to-oligomer transition. Because the oligomeric form is the major species and monomeric form has a negligible effect on SNARE-mediated vesicle fusion, we used the whole mixture without purification. Thus, concentrations of the protein applied in this work are given in monomeric units. The actual concentration of oligomers will be lower because many α-Syn mutant monomers participate in the assembly of a single oligomer. We obtained the same results by repeating the experiments with purified α-Syn mutant oligomers, confirming that our results were due to the oligomers present in oligomeric mixtures.

Functional α-Syn multimers, formed by the assembly of monomers upon binding to membranes, have been known to cluster synaptic vesicles (Diao et al., 2013; Wang et al., 2014), but this clustering does not interfere with vesicle fusion. However, α-Syn monomers at high concentrations of several μM range have been reported to cause vesicle clustering and subsequently to inhibit vesicle fusion (DeWitt and Rhoades, 2013; Diao et al., 2013). The concentration of monomers in α-Syn oligomeric mixtures in our experimental conditions was sub-micromolar concentration and thus vesicle clustering induced by the monomer itself would be negligible. The enhanced vesicle clustering by the presence of both oligomers and monomers cannot be excluded (Yoo et al., 2021; 2022). Because the monomer concentrations in the mixture were less than 250 nM; however, the vesicle clustering should dominantly occur by the oligomeric species. Importantly the experiments using purified oligomers confirmed that A30P and A53T oligomers inhibit vesicle fusion while E46K oligomers disrupt vesicle membranes in the presence of VAMP2 and anionic lipids, which is consistent with the results obtained by the oligomeric mixtures.

α-Syn is known to bind to curved negatively charged membranes, such as synaptic vesicles (Davidson et al., 1998; Eliezer et al., 2001). However, a recent study found that the E46K substitution disrupts its specificity for membranes, perhaps altering the distribution of membrane-bound α-Syn from synaptic vesicles to larger intracellular vesicles (Rovere et al., 2019). Indeed, E46K oligomers bind to planar SLBs by interacting with VAMP2 and reduce the mobility of the membrane, while other mutant oligomers do not. Membrane-bound α-Syn monomers were reported to form oligomers, which immobilize and disrupt the membrane by opening pores (Heo and Pincet, 2020; Reynolds et al., 2011). Thus, reduced membrane mobility by E46K oligomers in the

SLBs may result from their membrane disrupting activity. Additionally, we found that oligomers composed of E46K mutants drive vesicles to randomly fuse with one another, although whether E46K oligomers promote full fusion is unknown. Taken together, these results imply that E46K substitutions not simply increase the avidity of negatively charged large vesicles but also "try" to bind larger vesicles. Therefore, E46K oligomers may remodel and penetrate the presynaptic membrane, enhancing cell-to-cell transmission related to the pathological process of DLB, which is distinct from other mutant oligomers.

Note: Supplementary information is available on the Molecules and Cells website (www.molcells.org).

AUTHOR CONTRIBUTIONS
G.Y. and N.K.L. designed the experiments. G.Y., H.J.A., and S.Y. performed the experiments. G.Y. and N.K.L. wrote the manuscript.

CONFLICT OF INTEREST
The authors have no potential conflicts of interest to disclose.

ORCID
Gyeongji Yoo   https://orcid.org/0000-0001-5568-1737
Sanghun Yeou   https://orcid.org/0000-0002-4208-2601
Nam Ki Lee   https://orcid.org/0000-0002-6597-555X

REFERENCES

Agliardi, C., Meloni, M., Guerini, F.R., Zanzottera, M., Bolognesi, E., Baglio, F., and Clerici, M. (2021). Oligomeric α-Syn and SNARE complex proteins in peripheral extracellular vesicles of neural origin are biomarkers for Parkinson's disease. Neurobiol. Dis. *148*, 105185.

Alam, P., Bousset, L., Melki, R., and Otzen, D.E. (2019). alpha-synuclein oligomers and fibrils: a spectrum of species, a spectrum of toxicities. J. Neurochem. *150*, 522-534.

Bodner, C.R., Dobson, C.M., and Bax, A. (2009). Multiple tight phospholipid-binding modes of α-synuclein revealed by solution NMR spectroscopy. J. Mol. Biol. *390*, 775-790.

Burre, J., Sharma, M., and Sudhof, T.C. (2012). Systematic mutagenesis of alpha-synuclein reveals distinct sequence requirements for physiological and pathological activities. J. Neurosci. *32*, 15227-15242.

Burre, J., Sharma, M., and Sudhof, T.C. (2014). alpha-Synuclein assembles into higher-order multimers upon membrane binding to promote SNARE complex formation. Proc. Natl. Acad. Sci. U. S. A. *111*, E4274-E4283.

Burre, J., Sharma, M., Tsetsenis, T., Buchman, V., Etherton, M.R., and Sudhof, T.C. (2010). alpha-Synuclein promotes SNARE-complex assembly in vivo and in vitro. Science *329*, 1663-1667.

Cho, Y., An, H.J., Kim, T., Lee, C., and Lee, N.K. (2021). Mechanism of Cyanine5 to Cyanine3 photoconversion and its application for high-density single-particle tracking in a living cell. J. Am. Chem. Soc. *143*, 14125-14135.

Choi, B.K., Choi, M.G., Kim, J.Y., Yang, Y., Lai, Y., Kweon, D.H., Lee, N.K.,

and Shin, Y.K. (2013). Large alpha-synuclein oligomers inhibit neuronal SNARE-mediated vesicle docking. Proc. Natl. Acad. Sci. U. S. A. *110*, 4087-4092.

Choi, M.G., Kim, M.J., Kim, D.G., Yu, R., Jang, Y.N., and Oh, W.J. (2018). Sequestration of synaptic proteins by alpha-synuclein aggregates leading to neurotoxicity is inhibited by small peptide. PLoS One *13*, e0195339.

Conway, K.A., Harper, J.D., and Lansbury, P.T. (1998). Accelerated in vitro fibril formation by a mutant alpha-synuclein linked to early-onset Parkinson disease. Nat. Med. *4*, 1318-1320.

Conway, K.A., Lee, S.J., Rochet, J.C., Ding, T.T., Williamson, R.E., and Lansbury, P.T. (2000). Acceleration of oligomerization, not fibrillization, is a shared property of both alpha-synuclein mutations linked to early-onset Parkinson's disease: implications for pathogenesis and therapy. Proc. Natl. Acad. Sci. U. S. A. *97*, 571-576.

Conway, K.A., Rochet, J.C., Bieganski, R.M., and Lansbury, P.T. (2001). Kinetic stabilization of the alpha-synuclein protofibril by a dopamine-alpha-synuclein adduct. Science *294*, 1346-1349.

Danzer, K.M., Haasen, D., Karow, A.R., Moussaud, S., Habeck, M., Giese, A., Kretzschmar, H., Hengerer, B., and Kostka, M. (2007). Different species of alpha-synuclein oligomers induce calcium influx and seeding. J. Neurosci. *27*, 9220-9232.

Davidson, W.S., Jonas, A., Clayton, D.F., and George, J.M. (1998). Stabilization of alpha-synuclein secondary structure upon binding to synthetic membranes. J. Biol. Chem. *273*, 9443-9449.

Dettmer, U., Ramalingam, N., von Saucken, V.E., Kim, T.E., Newman, A.J., Terry-Kantor, E., Nuber, S., Ericsson, M., Fanning, S., Bartels, T., et al. (2017). Loss of native alpha-synuclein multimerization by strategically mutating its amphipathic helix causes abnormal vesicle interactions in neuronal cells. Hum. Mol. Genet. *26*, 3466-3481.

Dettmer, U., Selkoe, D., and Bartels, T. (2016). New insights into cellular α-synuclein homeostasis in health and disease. Curr. Opin. Neurobiol. *36*, 15-22.

DeWitt, D.C. and Rhoades, E. (2013). alpha-Synuclein can inhibit SNARE-mediated vesicle fusion through direct interactions with lipid bilayers. Biochemistry *52*, 2385-2387.

Diao, J.J., Burre, J., Vivona, S., Cipriano, D.J., Sharma, M., Kyoung, M., Sudhof, T.C., and Brunger, A.T. (2013). Native alpha-synuclein induces clustering of synaptic-vesicle mimics via binding to phospholipids and synaptobrevin-2/VAMP2. Elife *2*, e00592.

Eliezer, D. (2009). Biophysical characterization of intrinsically disordered proteins. Curr. Opin. Struct. Biol. *19*, 23-30.

Eliezer, D., Kutluay, E., Bussell, R., and Browne, G. (2001). Conformational properties of alpha-synuclein in its free and lipid-associated states. J. Mol. Biol. *307*, 1061-1073.

Fanning, S., Selkoe, D., and Dettmer, U. (2020). Parkinson's disease: proteinopathy or lipidopathy? NPJ Parkinsons Dis. *6*, 3.

Fuchs, J., Nilsson, C., Kachergus, J., Munz, M., Larsson, E.M., Schüle, B., Langston, J., Middleton, F., Ross, O.A., Hulihan, M., et al. (2007). Phenotypic variation in a large Swedish pedigree due to SNCA duplication and triplication. Neurology *68*, 916-922.

Furukawa, K., Matsuzaki-Kobayashi, M., Hasegawa, T., Kikuchi, A., Sugeno, N., Itoyama, Y., Wang, Y., Yao, P.J., Bushlin, I., and Takeda, A. (2006). Plasma membrane ion permeability induced by mutant alpha-synuclein contributes to the degeneration of neural cells. J. Neurochem. *97*, 1071-1077.

Fusco, G., Chen, S.W., Williamson, P.T.F., Cascella, R., Perni, M., Jarvis, J.A., Cecchi, C., Vendruscolo, M., Chiti, F., Cremades, N., et al. (2017). Structural basis of membrane disruption and cellular toxicity by alpha-synuclein oligomers. Science *358*, 1440-1443.

Fusco, G., Pape, T., Stephens, A.D., Mahou, P., Costa, A.R., Kaminski, C.F., Schierle, G.S.K., Vendruscolo, M., Veglia, G., Dobson, C.M., et al. (2016). Structural basis of synaptic vesicle assembly promoted by alpha-synuclein. Nat. Commun. *7*, 12563.

Giannakis, E., Pacífico, J., Smith, D.P., Hung, L.W., Masters, C.L., Cappai, R., Wade, J.D., and Barnham, K.J. (2008). Dimeric structures of α-synuclein bind preferentially to lipid membranes. Biochim. Biophys. Acta *1778*, 1112-1119.

Goedert, M. (2001). Alpha-synuclein and neurodegenerative diseases. Nat. Rev. Neurosci. *2*, 492-501.

Heo, P. and Pincet, F. (2020). Freezing and piercing of in vitro asymmetric plasma membrane by α-synuclein. Commun. Biol. *3*, 148.

Iwai, A., Masliah, E., Yoshimoto, M., Ge, N., Flanagan, L., De Silva, H.A.R., Kittel, A., and Saitoh, T. (1995). The precursor protein of non-Aβ component of Alzheimer's disease amyloid is a presynaptic protein of the central nervous system. Neuron *14*, 467-475.

Jackman, J.A. and Cho, N.J. (2020). Supported lipid bilayer formation: beyond vesicle fusion. Langmuir *36*, 1387-1400.

Jacobson, K., Liu, P., and Lagerholm, B.C. (2019). The lateral organization and mobility of plasma membrane components. Cell *177*, 806-819.

Jaqaman, K., Loerke, D., Mettlen, M., Kuwata, H., Grinstein, S., Schmid, S.L., and Danuser, G. (2008). Robust single-particle tracking in live-cell time-lapse sequences. Nat. Methods *5*, 695-702.

Jo, E.J., McLaurin, J., Yip, C.M., St George-Hyslop, P., and Fraser, P.E. (2000). alpha-synuclein membrane interactions and lipid specificity. J. Biol. Chem. *275*, 34328-34334.

Kim, D.H., Zhou, K., Kim, D.K., Park, S., Noh, J., Kwon, Y., Kim, D., Song, N.W., Lee, J.B., Suh, P.G., et al. (2015). Analysis of interactions between the epidermal growth factor receptor and soluble ligands on the basis of single-molecule diffusivity in the membrane of living cells. Angew. Chem. Int. Ed. Engl. *54*, 7028-7032.

Kim, H.Y., Cho, M.K., Kumar, A., Maier, E., Siebenhaar, C., Becker, S., Fernandez, C.O., Lashuel, H.A., Benz, R., Lange, A., et al. (2009). Structural properties of pore-forming oligomers of α-synuclein. J. Am. Chem. Soc. *131*, 17482-17489.

Kim, J.Y., Choi, B.K., Choi, M.G., Kim, S.A., Lai, Y., Shin, Y.K., and Lee, N.K. (2012). Solution single-vesicle assay reveals PIP2-mediated sequential actions of synaptotagmin-1 on SNAREs. EMBO J. *31*, 2144-2155.

Kruger, R., Kuhn, W., Muller, T., Woitalla, D., Graeber, M., Kosel, S., Przuntek, H., Epplen, J.T., Schols, L., and Riess, O. (1998). Ala30Pro mutation in the gene encoding alpha-synuclein in Parkinson's disease. Nat. Genet. *18*, 106-108.

Kumar, S.T., Donzelli, S., Chiki, A., Syed, M.M.K., and Lashuel, H.A. (2020). A simple, versatile and robust centrifugation-based filtration protocol for the isolation and quantification of alpha-synuclein monomers, oligomers and fibrils: towards improving experimental reproducibility in alpha-synuclein research. J. Neurochem. *153*, 103-119.

Lashuel, H.A., Petre, B.M., Wall, J., Simon, M., Nowak, R.J., Walz, T., and Lansbury, P.T. (2002). alpha-synuclein, especially the Parkinson's disease-associated mutants, forms pore-like annular and tubular protofibrils. J. Mol. Biol. *322*, 1089-1102.

Lee, Y., Kim, J., Kim, H., Han, J.E., Kim, S., Kang, K.H., Kim, D., Kim, J.M., and Koh, H. (2022). Pyruvate dehydrogenase kinase protects dopaminergic neurons from oxidative stress in Drosophila DJ-1 null mutants. Mol. Cells *45*, 454-464.

Li, J., Uversky, V.N., and Fink, A.L. (2001). Effect of familial Parkinson's disease point mutations A30P and A53T on the structural properties, aggregation, and fibrillation of human alpha-synuclein. Biochemistry *40*, 11604-11613.

Lou, X.C., Kim, J., Hawk, B.J., and Shin, Y.K. (2017). alpha-Synuclein may cross-bridge v-SNARE and acidic phospholipids to facilitate SNARE-dependent vesicle docking. Biochem. J. *474*, 2039-2049.

Maroteaux, L., Campanelli, J.T., and Scheller, R.H. (1988). Synuclein - a

neuron-specific protein localized to the nucleus and presynaptic nerve-terminal. J. Neurosci. *8*, 2804-2815.

McCormack, A., Keating, D.J., Chegeni, N., Colella, A., Wang, J.J., and Chataway, T. (2019). Abundance of synaptic vesicle-related proteins in alpha-synuclein-containing protein inclusions suggests a targeted formation mechanism. Neurotox. Res. *35*, 883-897.

Murphy, D.D., Rueter, S.M., Trojanowski, J.Q., and Lee, V.M.Y. (2000). Synucleins are developmentally expressed, and alpha-synuclein regulates the size of the presynaptic vesicular pool in primary hippocampal neurons. J. Neurosci. *20*, 3214-3220.

Musteikytė, G., Jayaram, A.K., Xu, C.K., Vendruscolo, M., Krainer, G., and Knowles, T.P.J. (2021). Interactions of α-synuclein oligomers with lipid membranes. Biochim. Biophys. Acta Biomembr. *1863*, 183536.

Narayanan, V. and Scarlata, S. (2001). Membrane binding and self-association of alpha-synucleins. Biochemistry *40*, 9927-9934.

Petrucci, S., Ginevrino, M., and Valente, E.M. (2016). Phenotypic spectrum of alpha-synuclein mutations: new insights from patients and cellular models. Parkinsonism Relat. Disord. *22* Suppl 1, S16-S20.

Pieri, L., Madiona, K., and Melki, R. (2016). Structural and functional properties of prefibrillar alpha-synuclein oligomers. Sci. Rep. *6*, 24526.

Polymeropoulos, M.H., Lavedan, C., Leroy, E., Ide, S.E., Dehejia, A., Dutra, A., Pike, B., Root, H., Rubenstein, J., Boyer, R., et al. (1997). Mutation in the alpha-synuclein gene identified in families with Parkinson's disease. Science *276*, 2045-2047.

Reynolds, N.P., Soragni, A., Rabe, M., Verdes, D., Liverani, E., Handschin, S., Riek, R., and Seeger, S. (2011). Mechanism of membrane interaction and disruption by α-synuclein. J. Am. Chem. Soc. *133*, 19366-19375.

Richter, R.P., Bérat, R., and Brisson, A.R. (2006). Formation of solid-supported lipid bilayers: an integrated view. Langmuir *22*, 3497-3505.

Robotta, M., Cattani, J., Martins, J.C., Subramaniam, V., and Drescher, M. (2017). Alpha-synuclein disease mutations are structurally defective and locally affect membrane binding. J. Am. Chem. Soc. *139*, 4254-4257.

Ross, C.A. and Poirier, M.A. (2004). Protein aggregation and neurodegenerative disease. Nat. Med. *10* Suppl, S10-S17.

Rovere, M., Powers, A.E., Jiang, H.Y., Pitino, J.C., Fonseca-Ornelas, L., Patel, D.S., Achille, A., Langen, R., Varkey, J., and Bartels, T. (2019). E46K-like α-synuclein mutants increase lipid interactions and disrupt membrane selectivity. J. Biol. Chem. *294*, 9799-9812.

Selvaraj, S. and Piramanayagam, S. (2019). Impact of gene mutation in the development of Parkinson's disease. Genes Dis. *6*, 120-128.

Spillantini, M.G., Crowther, R.A., Jakes, R., Hasegawa, M., and Goedert, M. (1998). alpha-synuclein in filamentous inclusions of Lewy bodies from Parkinson's disease and dementia with Lewy bodies. Proc. Natl. Acad. Sci. U. S. A. *95*, 6469-6473.

Spillantini, M.G., Schmidt, M.L., Lee, V.M.Y., Trojanowski, J.Q., Jakes, R., and Goedert, M. (1997). alpha-synuclein in Lewy bodies. Nature *388*, 839-840.

Stöckl, M.T., Zijlstra, N., and Subramaniam, V. (2013). alpha-Synuclein oligomers: an amyloid pore? Insights into mechanisms of α-synuclein oligomer-lipid interactions. Mol. Neurobiol. *47*, 613-621.

Stefanovic, A.N.D., Lindhoud, S., Semerdzhiev, S.A., Claessens, M., and Subramanian, V. (2015). Oligomers of Parkinson's disease-related alpha-synuclein mutants have similar structures but distinctive membrane permeabilization properties. Biochemistry *54*, 3142-3150.

Sun, J.C., Wang, L.N., Bao, H., Premi, S., Das, U., Chapman, E.R., and Roy, S. (2019). Functional cooperation of alpha-synuclein and VAMP2 in synaptic vesicle recycling. Proc. Natl. Acad. Sci. U. S. A. *116*, 11113-11115.

Tanaka, G., Yamanaka, T., Furukawa, Y., Kajimura, N., Mitsuoka, K., and Nukina, N. (2019). Biochemical and morphological classification of disease-associated alpha-synuclein mutants aggregates. Biochem. Biophys. Res. Commun. *508*, 729-734.

Tsigelny, I.F., Sharikov, Y., Wrasidlo, W., Gonzalez, T., Desplats, P.A., Crews, L., Spencer, B., and Masliah, E. (2012). Role of alpha-synuclein penetration into the membrane in the mechanisms of oligomer pore formation. FEBS J. *279*, 1000-1013.

van Meer, G., Voelker, D.R., and Feigenson, G.W. (2008). Membrane lipids: where they are and how they behave. Nat. Rev. Mol. Cell Biol. *9*, 112-124.

Volles, M.J. and Lansbury, P.T. (2002). Vesicle permeabilization by protofibrillar alpha-synuclein is sensitive to Parkinson's disease-linked mutations and occurs by a pore-like mechanism. Biochemistry *41*, 4595-4602.

Volles, M.J., Lee, S.J., Rochet, J.C., Shtilerman, M.D., Ding, T.T., Kessler, J.C., and Lansbury, P.T. (2001). Vesicle permeabilization by protofibrillar alpha-synuclein: implications for the pathogenesis and treatment of Parkinson's disease. Biochemistry *40*, 7812-7819.

Wakabayashi, K., Matsumoto, K., Takayama, K., Yoshimoto, M., and Takahashi, H. (1997). NACP, a presynaptic protein, immunoreactivity in Lewy bodies in Parkinson's disease. Neurosci. Lett. *239*, 45-48.

Wang, L.N., Das, U., Scott, D.A., Tang, Y., McLean, P.J., and Roy, S. (2014). alpha-Synuclein multimers cluster synaptic vesicles and attenuate recycling. Curr. Biol. *24*, 2319-2326.

Wang, W. (2005). Protein aggregation and its inhibition in biopharmaceutics. Int. J. Pharm. *289*, 1-30.

Wang, W., Nema, S., and Teagarden, D. (2010). Protein aggregation—pathways and influencing factors. Int. J. Pharm. *390*, 89-99.

Yeou, S. and Lee, N.K. (2022). Single-molecule methods for investigating the double-stranded DNA bendability. Mol. Cells *45*, 33-40.

Yoo, G., Shin, Y.K., and Lee, N.K. (2022). The role of α-synuclein in SNARE-mediated synaptic vesicle fusion. J. Mol. Biol. 2022 Aug 3 [Epub]. https://doi.org/10.1016/j.jmb.2022.167775

Yoo, G., Yeou, S., Son, J.B., Shin, Y.K., and Lee, N.K. (2021). Cooperative inhibition of SNARE-mediated vesicle fusion by α-synuclein monomers and oligomers. Sci. Rep. *11*, 10955.

Zakharov, S.D., Hulleman, J.D., Dutseva, E.A., Antonenko, Y.N., Rochet, J.C., and Cramer, W.A. (2007). Helical alpha-synuclein forms highly conductive ion channels. Biochemistry *46*, 14369-14379.

Zarranz, J.J., Alegre, J., Gomez-Esteban, J.C., Lezcano, E., Ros, R., Ampuero, I., Vidal, L., Hoenicka, J., Rodriguez, O., Atares, B., et al. (2004). The new mutation, E46K, of alpha-synuclein causes Parkinson and Lewy body dementia. Ann. Neurol. *55*, 164-173.